3070–3082 *Nucleic Acids Research, 2022, Vol. 50, No. 6* *Published online 8 March 2022*
https://doi.org/10.1093/nar/gkac151

G-quadruplex inducer/stabilizer pyridostatin targets *SUB1* to promote cytotoxicity of a transplatinum complex

Yinzhu Hou[1,2], Tieliang Gan[2], Tiantian Fang[1], Yao Zhao[1,*], Qun Luo[1,2], Xingkai Liu[1,2], Luyu Qi[1,2], Yanyan Zhang[1], Feifei Jia[1], Juanjuan Han[1], Shumu Li[1], Shijun Wang[3,*] and Fuyi Wang[1,2,3,4,*]

[1]Beijing National Laboratory for Molecular Sciences; CAS Key Laboratory of Analytical Chemistry for Living Biosystems; National Centre for Mass Spectrometry in Beijing, Institute of Chemistry, Chinese Academy of Sciences, No. 2 Zhongguancun North First Street, Haidian District, 100190 Beijing, P.R. China, [2]College of Chemical Science, University of Chinese Academy of Sciences, Yuquan Road, Shijingshan District, 100049 Beijing, P.R. China, [3]College of Traditional Chinese Medicine, Shandong University of Traditional Chinese Medicine, Jinshi Road, Lixia District, 250355 Jinan, P.R. China and [4]Key Laboratory of Mass Spectrometry Imaging and Metabolomics, Minzu University of China, National Ethnic Affairs Commission, Beijing 100081, P.R. China

Received November 03, 2021; Revised February 16, 2022; Editorial Decision February 17, 2022; Accepted February 20, 2022

ABSTRACT

Pyridostatin (PDS) is a well-known G-quadruplex (G4) inducer and stabilizer, yet its target genes have remained unclear. Herein, applying MS proteomics strategy, we revealed PDS significantly downregulated 22 proteins but upregulated 16 proteins in HeLa cancer cells, of which the genes both contain a number of G4 potential sequences, implying that PDS regulation on gene expression is far more complicated than inducing/stabilizing G4 structures. The PDS-downregulated proteins consequently upregulated 6 proteins to activate cyclin and cell cycle regulation, suggesting that PDS itself is not a potential anticancer agent, at least toward HeLa cancer cells. Importantly, *SUB1*, which encodes human positive cofactor and DNA lesion sensor PC4, was downregulated by 4.76-fold. Further studies demonstrated that the downregulation of PC4 dramatically promoted the cytotoxicity of *trans*-[$PtCl_2(NH_3)$(thiazole)] (*trans*-PtTz) toward HeLa cells to a similar level of cisplatin, contributable to retarding the repair of 1,3-*trans*-PtTz crosslinked DNA lesion mediated by PC4. These findings not only provide new insights into better understanding on the biological functions of PDS but also implicate a strategy for the rational design of novel multi-targeting platinum anticancer drugs via conjugation of PDS as a ligand to the coordination scaffold of transplatin for battling drug resistance to cisplatin.

GRAPHICAL ABSTRACT

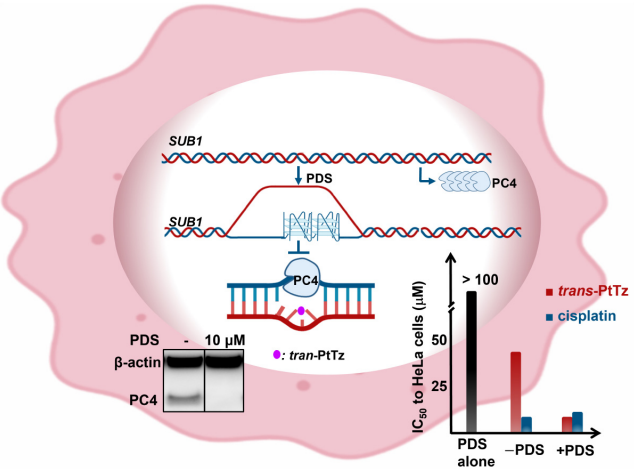

INTRODUCTION

G-quadruplexes (G4s) are stable secondary structures of nucleic acids, formed by hydrogen bonding of guanine bases in G-rich DNA or RNA sequences. Although studies on the formation and distribution of specific G4s in human chromatin are debatable and even controversial, it is commonly accepted that there are over 10 000 G4 potential sequences in human chromatin (1–3). G4s basically enrich in telomeres, somatic copy number alteration (SCNA) regions of cancer-associated genes. They were also widely detected in

*To whom correspondence should be addressed. Tel: +86 010 62529069; Email: fuyi.wang@iccas.ac.cn
Correspondence may also be addressed to Yao Zhao. Tel: +86 010 62529069; Email: yaozhao@iccas.ac.cn
Correspondence may also be addressed to Shijun Wang. Tel: +86 0531 89628750; Email: wsj@sdutcm.edu.cn

highly transcribed genes, especially regulatory regions such as promoters, splicing sites and 5'-untranslated regions (5′-UTR) (4,5). Since there are rich G4 potential sequences in oncogenes, e.g. *KRS* (6,7), *c-Myb* (8), *c-kit* (9), *BCL2* (10), *c-myc* (11,12) and *SRC* (1), G4s may serve as cancer biomarkers and be potential therapeutic targets. A number of G4 stabilizers, such as pyridostatin (13), Phen-DC3 (14) and BRACO19 (15), have been shown to be able to trigger the formation of DNA double-strand breaks (DSBs), resulting in activation of the DNA repair pathway (16,17). These implicate that G4 stabilizers may be used for cancer treatment, especially for the types of tumors of which the DNA damage repair system is impaired.

Pyridostatin (PDS) (Figure 1A) as a G4 inducer and stabilizer (13) mainly acts on nucleotide chains and can sustain the loading forces produced by DNA and RNA polymerases (18). Thus, DNA or RNA polymerases cannot open G4s, which as a consequence causes DNA DSBs. Moreover, PDS induces functional telomere abnormalities and generates DNA damages at specific genomic targets, exhibiting anti-proliferative activity (16). Due to the specific interactions between PDS and G4 patterns, PDS has also been derived as a tool for G4 enrichment, sequencing (19) and biological function research (20–22). What's more, it has been reported that due to the high binding affinity between PDS and G4s, PDS can displace certain G4-binding proteins, such as transcription factors (21,23), to disturb gene expression. However, to the best of our knowledge, the gene targets of PDS and the influence of PDS on genome-wide gene expression have been largely unexplored.

To this end, we herein used mass spectrometry (MS) based quantitative proteomics, which is widely applied to dissect molecular pathogenesis (24) and discover drug targets (25), to decipher the gene targets of PDS from the view of gene expression. Combining bioinformatics analysis, we discovered that PDS mainly down-regulated the expression of RNA binding proteins involved in RNA/mRNA splicing in HeLa cancer cells, which in turn up-regulated cell cycle related proteins, as a consequence, activating cyclin and cell cycle regulation. Importantly, we demonstrated for the first time that PDS down-regulated the expression of human positive cofactor PC4, significantly promoting the cytotoxicity of *trans*-[$PtCl_2(NH_3)$(thiazole)] (*trans*-PtTz) complex toward HeLa cells. The mechanism of this unique effect was further explored via molecular biological approaches and mass spectrometry analysis.

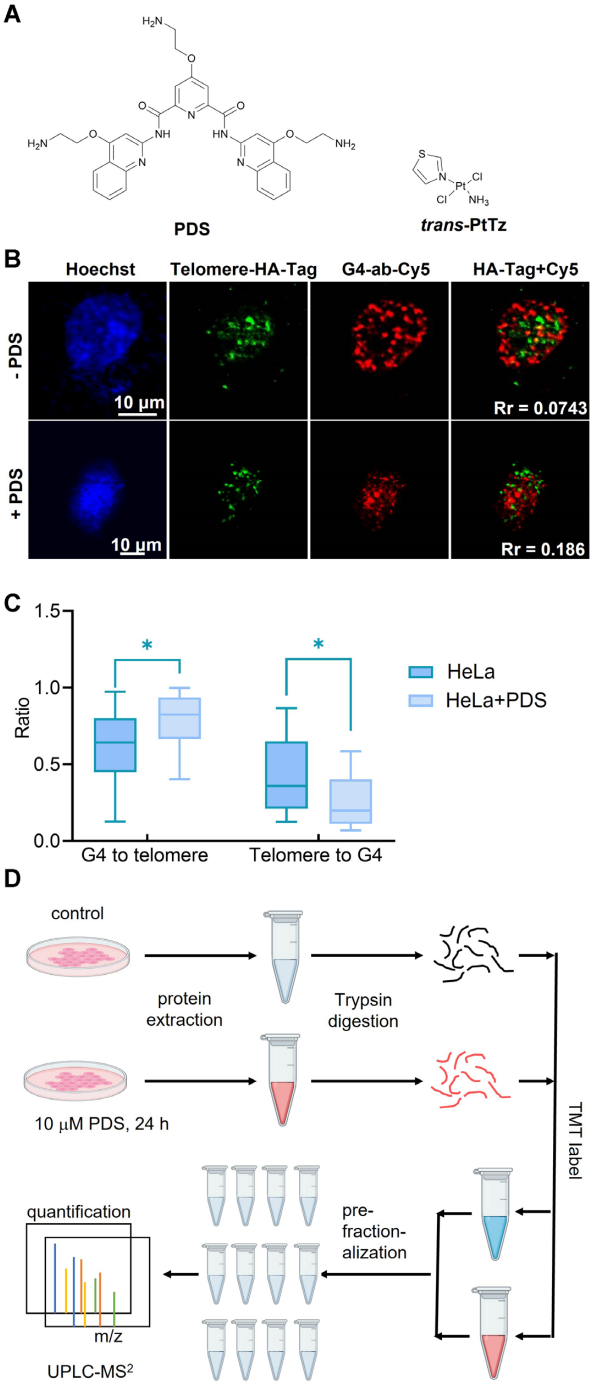

Figure 1. (**A**) The chemical structures of pyridostatin (PDS) and *trans*-[$PtCl_2(NH_3)$(thiazole)] (*trans*-PtTz). (**B**) Fluorescent co-localization of telomere and G4 DNA in HeLa cells transfected with Cas9-SunTag plasmids in the absence and the presence of PDS. Rr: Pearson's correlation coefficient; Blue indicates nucleus stained by DAPI, $\lambda_{ex} = 405$ nm, $\lambda_{em} = 425$–475 nm. Green indicates telomeres labeled with HA-tag conjugated with Cas9-SunTag, $\lambda_{ex} = 488$ nm, $\lambda_{em} = 500$–600 nm; red indicates G4 immunofluorescence signal with G4 antibody BG4, $\lambda_{ex} = 635$ nm, $\lambda_{em} = 650$–750 nm. (**C**) Statistic chart of co-localization ratio of G4 to telomere or telomere to G4 in HeLa cells transfected with Cas9-SunTag plasmids in the absence and the presence of PDS. There were 16 cells in HeLa-control group and 21 cells in HeLa + PDS group calculated for the co-localization ratio of G4 versus telomere. * indicates $P < 0.05$. (**D**) Workflow of mass spectrometric quantitative proteomics. Figure 1D was genenrated in bioRender.

MATERIALS AND METHODS

Chemicals and materials

Dithiothreitol (DTT) and Iodoacetamide (IAA) were purchased from J&K CHEMICA (China). Triethylammonium Bicarbonate and TMT10plex™ Isobaric Label Reagent Set were obtained from Thermo Scientific™. MS grade Acetonitrile and water were purchased from Fisher Chemical. Total Protein Extraction Kit was obtained from BestBio and Enhanced BCA Protein Assay Kit was from Beyotime. For antibodies, except BG4 (Ab00174-1.1) was purchased from Absolute Antibody Ltd, all other antibodies were purchased from Abcam. Cell Counting Kit-8 (CCK-8) was pur-

chased from MedChemExpress. Deionized water produced by Millipore system were used through the entire work.

Trans-[$PtCl_2(NH_3)$(thiazole)] (*trans*-PtTz) (Figure 1A) was synthesized by following the procedure reported previously (26). In brief, cisplatin was first synthesized according to the well-established step protocol (27). Then, cisplatin (255.52 mg), thiazole (141.7 μl, 98%, Innochem) and water (12.5 ml) were added into a round bottom flask and reacted at 70°C for 10 h. After that the mixture was cooled down to room temperature, and concentrated hydrochloric acid (2.1 ml, Sinopharm Chemical Reagent) was added and reacted at 80°C for further 12 h. Then the reaction mixture was incubated in an ice-water bath for 2 h for crystallization. Finally, the product was filtered, washed, dried and weighed to obtain pale yellow *trans*-PtTz (28.82 mg). Elemental analysis (%): Found C, 9.67; H, 1.67; N, 7.57; $C_3H_6Cl_2N_2PtS$ requires C, 9.79; H, 1.64; N, 7.61. ^{1}H NMR (400 MHz, acetonitrile-d_3) δ 9.45 - 9.31 (m, 1H), 8.23 (dd, J = 3.6, 0.9Hz, 1H), 7.64 (dd, J = 3.6, 2.4 Hz, 1H), 3.36 (s, 3H) (Supplementary Figure S1). ESI-MS (m/z): $C_3H_5ClN_2PtS$ ([M-Cl]$^+$) calculated: 331.96, found: 331.96.

Cell culture

Human HeLa cervical cancer cells (National Infrastructure of Cell Line Resource, Beijing, China) were cultured in DMEM (Dulbecco's Modifed Eagle's Medium, Gibco), which contained 10% fetal bovine serum (FBS, Gibco) and 1% penicillin-streptomycin (GE Heathcare Life Sciences). All cells were cultured in 5% CO_2 in a 37°C incubator.

Confocal laser scanning microscopy fluorescence imaging

To localize PDS-induced G4s in cells, we applied Cas9-SunTag technique to image telomeres while applying G-quadruplex antibodies BG4 (28) to visualize G4s, including DNA/RNA G4s, by confocal laser scanning microscopy (CLSM) fluorescence imaging. Cas9-SunTag is one of fluorescence probes for labeling specific DNA sequences or gene loci in living cells (29). It links 24 polypeptide scaffolds at the C-terminus of dCas9 protein, allowing dCas9 to recruit 24 sfGFP proteins into the hybridization sites of sgRNA and genomic DNA so as to enhance significantly fluorescence signal of DNA targets. However, we found that the GFP fluorescence signal derived from dCas9-SunTag at telomere regions was largely quenched due to G4-BG4 immunostaining (30). Thus, we used immunostaining to illuminate telomeres via HA-tag expressed by the HA-tagged scfv-GCN4-GFP-VP64 plasmid (29). In this case, the superposition of the antibody to BG4 and the antibody to the HA-tag can be used to judge whether and how much G4s co-localize with telomeres.

To achieve the co-localization imaging, HeLa cells were seeded in confocal dish (ThermoFisher Scientific) and grew in DMEM in 5% CO_2 in a 37°C incubator. When the cell density reached about 70%, the dCas9-SunTag10×-v4, scfv-GCN4-GFP-VP64 and sgTelo plasmids, which were kindly provided by Professor Yu Zhang at National Institute of Biological Sciences as gifts, were simultaneously transfected with Lipo3000 transfection reagent (ThermoFisher Scientific). After 48 h, the cells were treated with cold methanol-acetic acid fixative for 10 min, washed three times with phosphate-buffered saline (PBS), permeabilized with 0.1% Triton-X100/PBS on the decolorizing shaker for 30 min and then blocked with 5% BSA/PBS solution at 37°C for 1 h. Thereafter, the cells were incubated with the rabbit polyclonal primary antibody to HA tag (Abcam, ab9110) and the G4 primary antibody BG4 (Absolute Antibody Ltd, Ab00174-1.1) at 37°C for 1 h, washed 5 times with buffer (0.2% BSA/PBS), then incubated with the donkey anti-rabbit secondary antibody conjugated with Alexa Fluor® 488 (Abcam, ab150073) to ab9110 and the goat anti-mouse secondary antibody conjugated with Cy5 (ab136127) to ab150073 at 37°C for 1 h, followed by washing three times with buffer prior to LSCM imaging. The excitation and emission wavelength were 488 nm and 500–600 nm, 635 nm and 650–750 nm for Alexa Fluor®488 and Cy5, respectively.

Quantitative proteomics analysis

Protein extraction. HeLa cells culturing in DMEM as described above were divided into control group and PDS treated group, and incubated in the absence and the presence of 10 μM PDS, respectively, at 37°C for 24 h. The cells were then individually harvested, lysed on ice and extracted whole cell proteins by total protein extraction kit (BestBio). The concentration of raw protein extracts was measured by BCA Kit (Beyotime).

Protein digestion. Exactly 300 μg extracted proteins in lysis buffer from each group was transferred to 1.5 ml low protein binding microcentrifuge tube (Thermo Fisher Scientific), and DTT was added at a final concentration of 5 mM. The resulting mixture reacted at 37°C for 1 h. Then IAA was added at a final concentration of 10 mM to alkylate the cysteine residues by incubation at 25°C for 45 min in the dark. After diluted 3 times with 50 mM Tris-HCl (pH 8.0), 6 μl of 1 μg/μl trypsin was added to digest proteins at 25°C overnight. Thereafter, the peptides were desalted in C18 cartridge (Waters Sep-Pak part No. WAT023590). The C18 column was firstly activated by 1 ml of acetonitrile (ACN) and 1 ml of 50% (vol/vol) ACN/H_2O with 0.1% (vol/vol) formic acid (FA) successively, followed by equilibration with 3 ml of 0.1% (vol/vol) TFA (trifluoacetic acid) in H_2O. Then the peptides were loaded to the C18 column, and the desalting was achieved by washing the column with 3 ml of 0.1% (vol/vol) TFA and 1 ml of 1% (vol/vol) FA. The peptide residues were sequentially eluted by 1 ml of 50% (vol/vol) ACN and 1 ml of 80% (vol/vol) ACN/H_2O, and the eluents were merged, followed by drying in vacuum centrifuge (CentriVap, ThermoFisher Scientific).

Stable isotopic labeling. Exactly 100 μg peptide residues of each group was re-dissolved in 50 mM HEPES (pH 8.5) to a final concentration of 1 μg/μl and labeled with TMT labeling reagent (Thermo Fisher Scientific). The sample of the control group was labeled with 130N, and the PDS group was labeled with 129C. The labeling reaction was initialized by incubation at room temperature for 1 h and quenched by 8 μl of 5% hydroxylamine. The labeled peptides derived from control group and PDS group were then equivalently mixed, desalted and dried as described above.

HPLC pre-fractionation. The labeled peptide mixture was re-dissolved in 100 μl 2% (vol/vol) ACN/H_2O containing 4.5 mM ammonium formate (pH 10) for basic reverse-phase chromatography pre-fractionation. Aliquot (97 μl) of peptide mixture was loaded to HPLC (Agilent Technologies 1260 infinity) with Agilent ZORBAX 300 Extend-C18 column. The mobile phase A was 4.5 mM ammonium formate in 2% (vol/vol) ACN/H_2O (pH 10), and phase B 4.5 mM ammonium formate in 90% (vol/vol) ACN/H_2O (pH 10). The gradient started with 0% B until 7 min and continuously increased to 16% B at 13 min, 40% B at 73 min, 44% B at 77 min, and 60% B at 82 min and kept until 96 min, then increase to 90% B at 100 min. The flow rate was 1 ml/min. The fractions were collected chronologically into twelve tubes from 3 to 96 min, lyophilized and re-dissolved with H_2O containing 0.1% FA to a 500 ng/μl concentration for mass spectrometric analysis.

NanoLC-MS/MS analysis. Mass spectrometric quantification was performed on an Orbitrap Fusion Lumos mass spectrometer coupled with an EASY-nLC 1200 nanoUPLC system equipped with an Acclaim™ PepMap™ 100 pre-column (20 mm × 75 μm, 3 μm) and an Acclaim™ PepMap™ RSLC C18 analytical column (150 mm × 75 μm, 2 μm). The UPLC mobile phase A was water containing 0.1% FA, and phase B 80% (vol/vol) methanol/water containing 0.1% FA. The UPLC gradient started with 2% B and increased to 7% at 7 min, then to 20% at 69 min, 35% at 90 min and sharply to 95% within 5 min, remained for 4 min, and finally decreased to 2% within 8 min and remained for 3 min. Aliquot (1 μl) of each HPLC fraction described above was injected to UPLC, and the elution from the analytical column was directly infused to the mass spectrometer for MS/MS analysis. The detail of the parameters of the MS/MS analysis are listed in Supplementary Table S1.

Protein identification and quantification. Raw MS/MS data were searched in Proteome Discoverer (Thermo Scientific, version 2.3) database for peptide and protein identification. Sequest HT search engine was used for peptide-spectrum matching (PSM). The dynamic modifications were oxidation at methionine, methylation at lysine, glutarnine and arginine, acetylation at lysine and serine, phosphorylation at serine, threonine and tyrosine, and TMT labeling at lysine. The static modifications were carbamidomethylation at cysteine and TMT labeling at N-terminus of peptides. The quantitative results were normalized based on the total peptide amount in each group. Only proteins identified with false discovery rate (FDR) <0.01, P-value <0.05 and abundance ratio <0.833 or >1.20 were included for further analyses.

The entire quantitative proteomics analysis was carried out in three independent replicates.

Bioinformatics analysis

Ingenuity Pathway Analysis (IPA) (QIAGEN Digital Insights) and STRING (Ver. 11.5, https://cn.string-db.org) program were used to stimulate molecular activity and to map the protein–protein interaction (PPI) network of the differentially expressed proteins (DEPs) subjected to PDS treatment.

Western blot assay

The expression level of PC4 in HeLa cells in the absence and the presence of PDS were measured by western blotting with β-actin as an internal control protein. HeLa cells were cultivated in the presence of 0, 2 and 10 μM PDS, respectively, for 24 h. The cells were harvested for extracting whole cell proteins using Mammalian protein extraction reagent (Thermo Scientific). Then the BCA assay was performed to determine the concentration of each protein extract. Aliquot (60 μg) of protein extract was boiled at 95°C for 5 min with the gel-loading buffer (4 × LDS, Genscript, Nanjing, China), and separated with a 10% gradient SDS-PAGE gel (Genscript) at 110 V for 40 min. Then the separated proteins were transferred to a PVDF membrane (Millipore, 0.2 μm). The membrane was blocked in 5% nonfat dry milk (Biofroxx) dissolved in 0.1% TBST at room temperature for 1 h, followed by incubated with primary antibodies (ab8227 for β-actin, ab72132 for PC4) in appropriate dilutions for 1 h, washed by blocking buffer for 30 min, incubated with the secondary antibody (ab7090) for 1 h, washed as described before and washed with 0.1% TBST for 5 min. The protein bands were visualized by chemiluminescent HRP substrate (Millipore), and the optical densities were determined by ImageJ.

Time of flight secondary ion mass spectrometry (ToF-SIMS) imaging

For ToF-SIMS imaging, HeLa cervical cancer cells were seeded on silicon wafer and cultivated to a density of 80% and divided into three groups: blank group (cells were cultivated without both PDS and *trans*-PtTz), control group (cells were treated with 25 μM *trans*-PtTz for 24 h) and PDS group (cells were pretreated with 10 μM PDS for 24 h and then treated with 25 μM *trans*-PtTz for another 24 h). The cells were fixed with pure pre-cooled ethanol for 20 min, then washed three times with PDS, followed by washing three times with ammonium acetate (150 mM, pH 7.4), then quickly frozen by liquid N_2 and transferred intermediately into a lyophilizer (LGJ-12, Beijing Songyuanhuaxing Technology Develop Co., Ltd) at 193 to 208 K for freeze-drying overnight.

ToF-SIMS imaging was carried out with a ToF-SIMS 5 instrument (ION-ToF GmbH, Münster, Germany) equipped with a 30 keV liquid metal primary ion source. The high-lateral-resolution (ca. 200–300 nm) images of cells were recorded using Bi_3^+ primary ion gun. For imaging, signals were collected with 256 × 256 pixels in negative mode and the scanning area was 250 μm × 250 μm. The scan times of each sample were exactly 3000 to obtain high quality images. The images of various ions were collected and plotted with the Surface Lab software (version 6.4 ION-ToF GmbH). The mass to charge ratio (m/z) was calibrated using the signals of C^-, CH^-, CH^{2-}, C^{2-}, C_2H^-. The image of Pt was constructed by sum of signals of $[^{194}PtCN]^-$, $[^{195}PtCN]^-$ and $[^{196}PtCN]^-$ ions (31,32), and the image of total and PO_3^- was used to profile the shape of cells. Shift correction was applied by the software for all the images. Region of interest (ROI) were created for 20 cells in each sample, and the Pt signal of each cell was normalized to total signal for further statistics analysis.

Inductively coupled plasma mass spectrometry (ICP-MS)

For ICP-MS analysis, HeLa cells were cultured in DMEM as described above and the group set was the same as ToF-SIMS imaging. Cells were individually collected for each group, and DNA was then extracted by Genomic DNA Mini Preparation Kit with Spin Column (Beyotime). The concentration of DNA in each sample was detected by NanoDrop (ThermoFisher Scientific) before the concentration of Pt was detected by ICP-MS (Agilent 7700). The experiment was repeated three times independently. The Pt concentrations of each group were represented as the numbers of Pt atom in 10^6 bp (base pair).

In vitro anti-proliferative assay

For the measurement of cytotoxicity of *trans*-[$PtCl_2(NH_3)$(thiazole)] (*trans*-PtTz) with or without PDS pre-treatment, HeLa cells were cultured as described above, and seeded into and grew in a 96-well plate at 37°C to achieve 80–90% density in DMEM medium in the absence of PDS and in the presence of 2 or 10 μM of PDS, respectively. After cultured for 24 h, the cells were wished twice with PBS, and 200 μl medium containing 0, 2, 8, 30, 50, 70, 100, 180 or 200 μM of *trans*-PtTz was added to each well. After 24 h of incubation at 37°C, each well was added 10 μl CCK-8 (MedChemExpress) reagents and incubated for further 3 h. Then, the absorbance at 450 nm was measured and the IC_{50} value, which is the concentration of tested complex inhibiting 50% growth of cells, were calculated accordingly.

For comparison, the 24 h IC_{50} values against HeLa cells of cisplatin, which is the structural isoform of transplatin and one of the widely used anticancer metallodrugs for treatment of solid tumors, in the absence and in the presence of 2 μM or 10 μM of PDS were measured following the similar procedure described above. The concentration gradient of cisplatin was 0, 1, 10, 15, 20, 30, 50, 70 and 100 μM. Meanwhile, the 24 h IC_{50} value of PDS alone toward HeLa cells was also determined with a concentration gradient of 0, 2, 10, 20, 30, 40, 50, 60, 70, 100, 120, 180 and 200 μM.

qPCR measurement

HeLa cells were divided into control group and PDS treated group, and incubated in the absence and the presence of 10 μM PDS, respectively, at 37°C for 24 h. The cells were then lysed with Trizol (Thermo Scientific) and the whole RNA were extracted following the instructions of the manufacturer. The qPCR measurement was performed by Sangon Biotech with Maxima Reverse Transcriptase (Thermo Scientific) and Stepone Plus Real-Time PCR system (ABI, Foster, CA, USA). β-Actin was used to be the internal reference. The primer sequences for qPCR were TTGGGAAAATGAGGTACGTTAGT (SUB1-F), TTTTCTTCCTGGTTTCATTTCA (SUB1-R); GATGTC GCTTACAGAGTCACCA (COL5A1-F), TTGGCTTT CACAGTTGTTAGGA (COL5A1-R); CTCCACTTTC CAGCACATCC (THRAP3-F), CTCTTACCCACAGG GCTCTTT (THRAP3-R); GGCGCACCAGGCTTATTA (ARL6IP4-F), GGTGGCTTGCTTGTTGA (ARL6IP4-R); TGAAGCTGGTCTACTGTGCTC (GPC1-F), CCCA GAACTTGTCGGTGATGA (GPC1-R) and TAGTTG CGTTACACCCTTTCTTG (β-actin-F), TCACCTTCAC CGTTCCAGTTT (β-actin-R).

RESULTS

Fluorescence imaging of target genes of PDS

Since telomeres contain a large number of rich G4 potential sequences which may be the target of PDS, we first applied confocal laser scanning microscopy (CLSM) to co-localize telomeres and G4s in single cells to elucidate this hypothesis. We utilized the Cas9-SunTag technique combined with HA-tag immunostaining (29) to image telomeres while visualizing G4s by using G-quadruplex antibodies BG4 (28) in human HeLa cervical cancer cells in the absence and the presence of PDS. The repeating peptide array termed SunTag was genetically fused to the endonuclease-deficient Cas9 (dCas9) protein (29) and recruited multi-copies of scFv-GCN4-GFP-HA tag to illuminate telomeres directed by telomere-specific guide RNA (gRNA). In this case, the superposition ratio of BG4 signal and HA-Tag signal was used to determine the co-localization ratio of G4 to telomere or telomere to G4. As shown in Figure 1B, PDS induced formation of G4 in telomere regions as evidenced by the increased Pearson's correlation coefficient from 0.0743 to 0.186 between the fluorescence signals of telomere and G4 in the single cell. However, the statistic results based on more cells indicated that after PDS treatment, the co-localization ratio of telomere to total G4 decreased, though the co-localization ratio of G4 to telomere increased (Figure 1C). This indicated that more G4s formed on non-telomeric regions in the presence of PDS. In other words, PDS mainly targeted non-telomeric nucleic acid sequences, consistent with previous reports (13,16).

Protein profiling of HeLa cells subjected to PDS treatment

Next, we applied mass spectrometry (MS) based quantitative proteomics to profile the protein expression of HeLa cells subjected to PDS treatment (Figure 1D). Three independent MS-based quantitation experiments on HeLa cells with and without 10 μM PDS treatment allowed us to identify a total of 4316 proteins (Figure 2A), of which 674 proteins have a statistical significance ($P < 0.05$) (Figure 2B). The search results based on the MS/MS data are provided in Supplementary Table S2. To identify the differentially expressed proteins (DEPs) in HeLa cells exposed to 10 μM PDS for 24 h, the protein profiles between the two data sets were compared. We found that the abundance ratio (AR) of the 637 proteins expressing in the PDS treated group versus the control group were between 0.667 and 1.50, indicating that the expression of major proteins (637/674) was not significantly affected by PDS (blue dots in Figure 2B). Notably, among the 674 proteins, only four proteins are directly related to telomere and their AR values were not significantly changed, suggesting that PDS has little effect on the expression of telomere-related proteins, consistent with the fluorescence co-localization results described above.

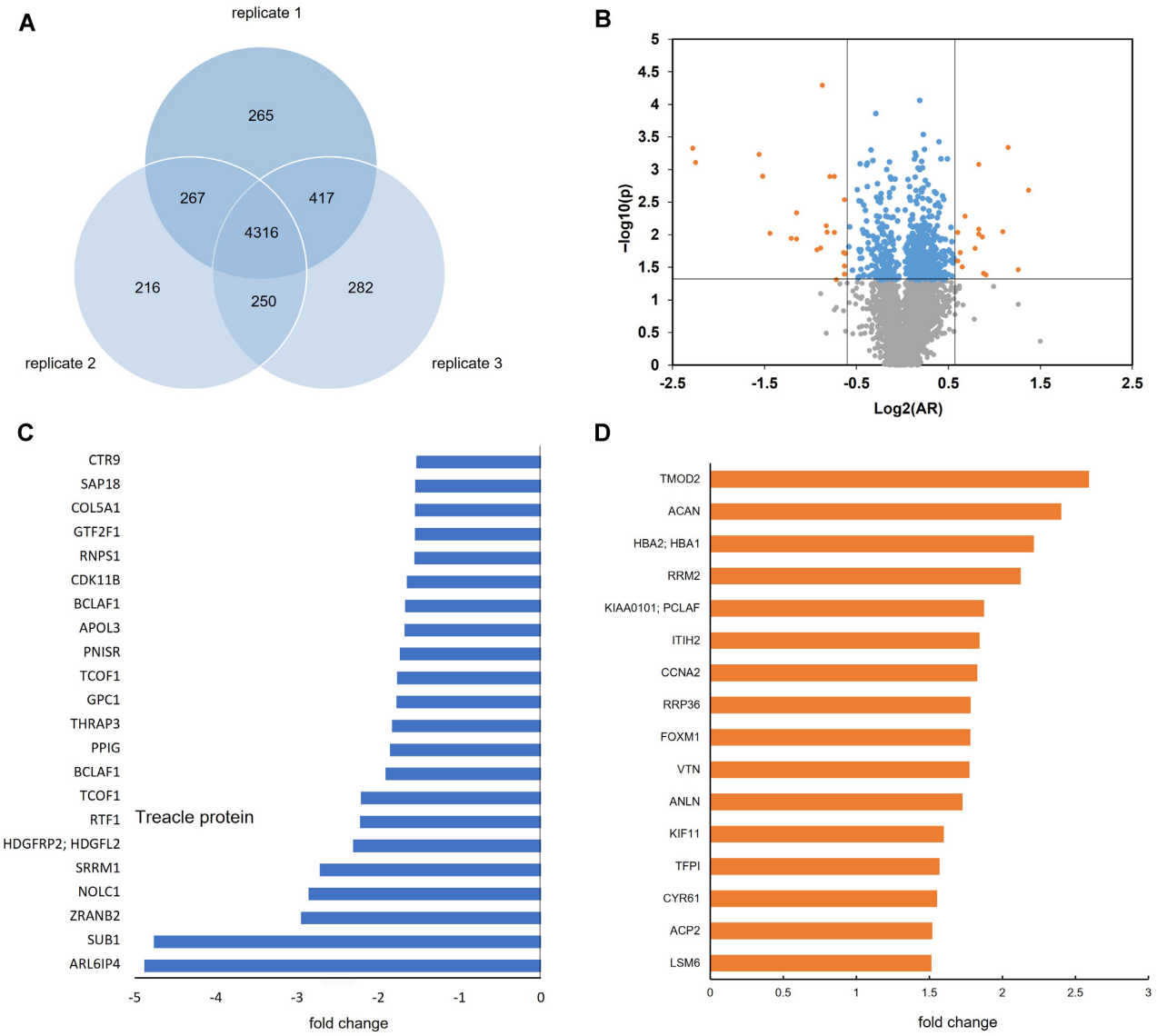

Figure 2. (**A**) Venn diagram of the numbers of the proteins identified in three parallel experiments, showing 4316 proteins found in common. (**B**) Volcano map of the proteins commonly detected in three replicates. The lower panel represents proteins with $P > 0.05$, upper middle panel represents proteins with $P < 0.05$ and $0.667 < AR < 1.50$, and upper left and upper right panels represent proteins with $P < 0.05$ and $AR < 0.667$, and $P<0.05$ and $AR > 1.50$, respectively. (**C** and **D**) The significantly differential expressed proteins (DEPs) with change fold < -1.5 (C) or > 1.50 (D) in HeLa cells subjected to PDS treatment.

The fold change (FC), which is equal to AR of a protein when AR > 1, but to negative reciprocal of AR when AR < 1, was used to describe how much a protein is up- or down-regulated. As shown in Supplementary Figure S2, 159 proteins were upregulated with FC > 1.2, and 82 proteins downregulated with FC < -1.2 in HeLa cells subjected to PDS treatment. Among them, 22 proteins were significantly down-regulated, and 16 proteins remarkably up-regulated with a |FC|>1.5 (Figure 2C,D). The Gene Ontology (GO) information summarized in Supplementary Table S3 indicated that most of the differentially expressed proteins (DEPs) due to PDS treatment are DNA/RNA binding proteins, and involved in cellular metabolism, cell organization and biogenesis, and cell differentiation and proliferation.

As a G4 inducer and stabilizer, it is commonly accepted that PDS regulated gene expression mainly through inducing/stabilizing the formation of G4s both in DNA and RNA (22). Thus, we searched endogenous G4 structures in the genes of all DEPs induced by PDS based on the latest published ChIP-Seq data (GSE 145090) with the use of G4 structure-specific antibody (33). We discovered that 80% (16) of the 20 down-regulated genes, among which the gene *TCOF1* simultaneously encodes treacle protein and its isoform 7, and the gene *BCLAF1* encodes Bcl-2-associated transcription factor 1 and its isoform 3 (Figure 2C and Supplementary Table S3), naturally form G4 structures, and that 81% (13) of the 16 genes have G4 structures in their promoter regions (Figure 3A). Moreover, we found that 43% (6) of the 14 up-regulated genes also have endogenous G4s in

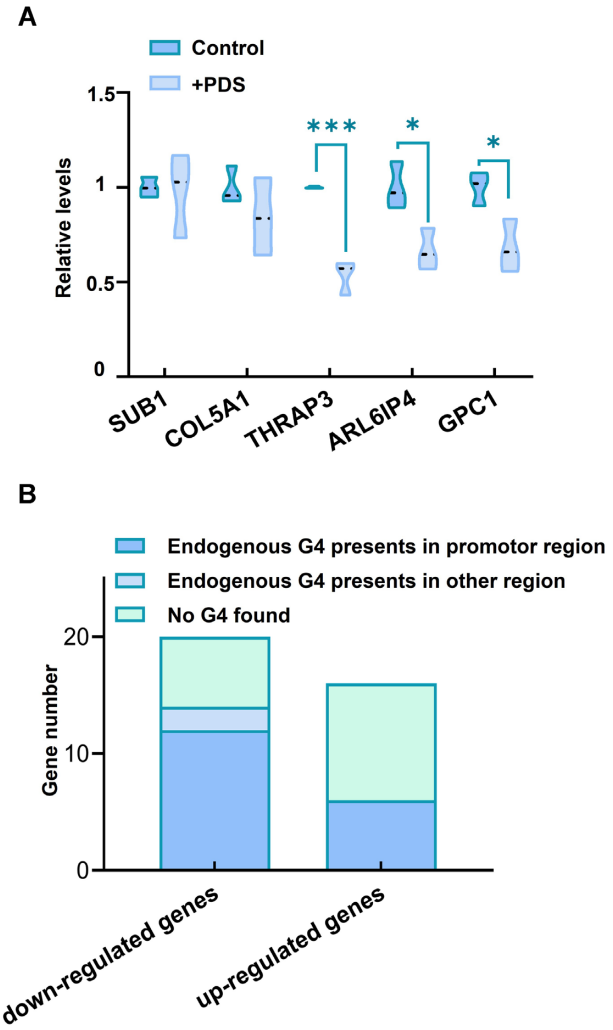

Figure 3. (**A**) The regulation of 10 μM PDS on the transcription level of five selected genes; * indicates $P < 0.05$ and *** $P < 0.001$. (**B**) The numbers of the genes of which the expression was found in this work to be down-regulated or up-regulated by PDS, and in which G4 structures present or not found as reported in previous G4 ChIP-Seq data.

their promoter regions, though the PDS-upregulated genes have a much lower proportion of naturally formed G4s than the PDS-downregulated genes.

Next we applied Quadruplex forming G-Rich Sequences (QGRS) mapper (34) to count the potential G4 sequences in the 36 PDS regulated genes (Table 1). Again, both the PDS regulated genes contain a significant number of potential G4 sequences in their transcribed sequences and promoter regions. Similarly, the downregulated genes have a higher average number of G4 potential sequences than the upregulated ones. However, the number of QGRS in PDS-downregulated gene is not directly proportional to the reduction in the expression of the gene due to PDS treatment (Supplementary Figure S3). With regard to this, a possible reason may be that PDS could induce/stabilize G4 structures in either genetic DNA or mRNA, regulating the expression of the targeted genes at either transcription or translation stage, or at both (33). Furthermore, the location of PDS targeting sites, for example, at promoter region, impacts gene expression more than other PDS potential targeting sites.

To figure out whether PDS inhibits the expression of its target genes at transcription level or translation level, we selected *SUB1*, which encodes a positive transcription cofactor PC4, to perform qPCR measurement. As shown in Figure 3B, PDS had little effect on the transcription level of *SUB1*. We further extended qPCR measurement to two pair of genes, *COL5A1* and *THRAP3*, and *ARL6IP4* and *GPC1*, which have the largest number of potential G4 sequences in the transcribed sequences and the promoter region, respectively. We found that the transcription of these four genes except for *COL5A1* were downregulated significantly by PDS, though *COL5A1* has the largest number of potential G4. These again indicate that the number of G4 structures presenting in a gene is not the mere determinant for PDS regulation on its expression.

To elucidate the mechanism of PDS upregulating gene expression, we mapped the PPI network of the 16 up-regulated proteins with FC > 1.5 by STRING. We found that they were clustered into two groups by their biological functions: cellular component organization and regulation of cell cycle (Supplementary Figure S4). The cellular component organization was triggered by the acute phase responses of cells to PDS stimulation, in which proteins ACAN, VTN, LSM6, RRP36, CYR61, TMOD2, ACP2 and HBA2 are involved. While RRM2, ANLN, CCNA2, FOXM1, KIF11 and KIAA0101 appear to activate the regulation of cell cycle. These are unexpected because PDS was thought to be able to induce the formation of G4s, leading to formation of DSBs and probably activating DNA-damage checkpoint signaling and cell cycle arrest (16).

To further find out what resulted in the upregulation of cell cycle related proteins during the PDS treatment, the molecule activity predictor (MAP) simulation in IPA program was performed. We found that all the PDS downregulated proteins with FC < 1.0 led to the activation of three transcription factors: FOXO1, MITF and TP63, which subsequently upregulated the downstream proteins including ANLA, KIF11, CCNA2 and RRM2 (Figure 4 and Supplementary Table S4) as well as FOXM1 and KIAA0101 which are co-expressed with the four cell-cycle related proteins as shown in Supplementary Figure S4.

PDS promotes cytotoxicity of *trans*-[$PtCl_2(NH_3)$(thiazole)] by silencing *SUB1*

It is notable that among the PDS down-regulated genes we identified, *SUB1*, which encodes the human nuclear positive cofactor PC4, had the second highest fold-change (4.76) (Figure 2C), evidenced further by Western Blot assay which showed that 10 μM PDS almost silenced this gene completely (Figure 5A). Endogenous PC4 is an abundant single-strand DNA-binding protein that stimulates activator-dependent class II gene transcription. It specifically recognizes G4 structure and DNA lesions (35–38), thereby activating double-strand break (DSB) repair by stimulating the joining of non-complementary DNA ends, and promoting genome stability (39). Our previous study revealed that PC4 recognized and specifically bound to 1,3-intrastrand crosslinked DNA by *trans*-[$PtCl_2(NH_3)$(thiazole)] (*trans*-

Table 1. The Quadruplex forming G-Rich Sequences (QSRS) in the genes of which the expression was significantly regulated by PDS.

Down-regulated Genes										
Gene Name	*ARL6IP4*	*SUB1*	*ZRANB2*	*NOLC1*	*SRRM1*	*HDGFRP2*	*RTF1*	*TCOF1*	*BCLAF1*	*PPIG*
QGRS in full gene sequence	46	389	41	84	133	332	428	420	60	203
QGRS in promoter sequence	28	11	9	17	22	8	15	8	6	11
Gene Name	*THRAP3*	*GPC1*	*PNISR*	*APOL3*	*CDK11B*	*RNPS1*	*GTF2F1*	*COL5A1*	*SAP18*	*CTR9*
QGRS in full gene sequence	487	425	80	163	185	105	128	1958	57	119
QGRS in promoter sequence	17	26	5	22	26	25	17	22	10	9
Up-regulated Genes										
Gene Name	*TMOD2*	*ACAN*	*HBA2*	*RRM2*	*KIAA0101*	*ITIH2*	*CCNA2*	*RRP36*	*FOXM1*	*VTN*
QGRS in full gene sequence	223	408	6	617	93	177	13	61	105	31
QGRS in promoter sequence	6	9	9	17	8	12	4	20	18	20
Gene Name	*ANLN*	*KIF11*	*TFPI*	*CYR61*	*ACP2*	*LSM6*				
QGRS in full gene sequence	165	168	151	13	85	66				
QGRS in promoter sequence	12	8	1	9	14	5				

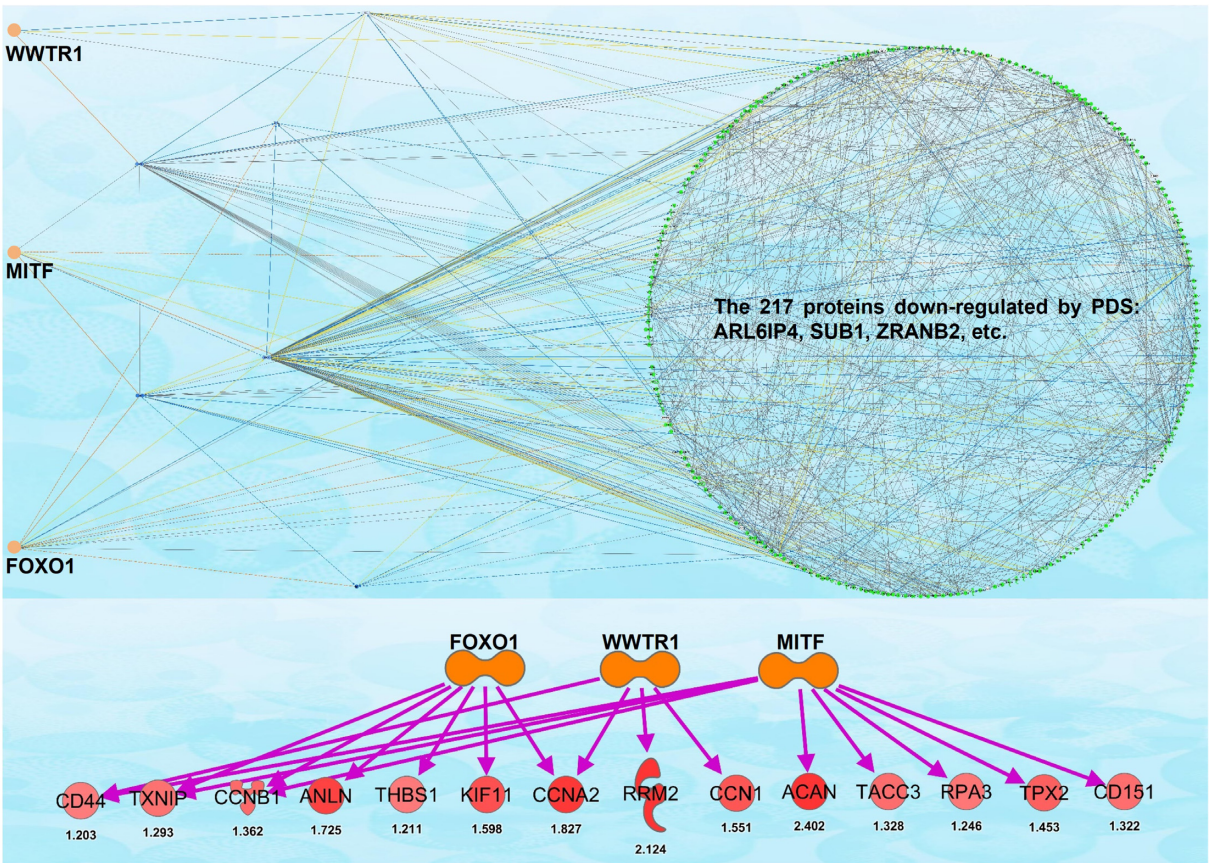

Figure 4. The molecule activity predictor (MAP) simulation of 217 PDS down-regulated proteins (green dots) with FC < 1 performed by IPA. It shows that the down-regulated proteins lead to the activation of three transcription factors: WWTR1, MITF and FOXO1, which subsequently up-regulate the downstream proteins listed in the bottom with MS-detected fold-changes below.

PtTz), a cytotoxic transplatinum complex (40) (Figure 1A), and may play a crucial role in cellular response to DNA damage by *trans*-PtTz (36). These together inspired us to investigate how the PDS-induced downregulation of PC4 would impact the cytotoxicity of *trans*-PtTz which is believed to target genomic DNA as an anticancer agent (41).

To address this issue, we first measured the IC_{50} of PDS alone toward HeLa cells. As shown in Supplementary Figure S5, the IC_{50} of PDS was >100 μM for 24 h treatment, though 10 μM PDS could cause ∼50% HeLa cell death when the incubation time was extended to 72 h. This indicates that PDS alone is a low cytotoxic compound. Next, we evaluated the cytotoxicity of *trans*-PtTz toward HeLa cells when PDS co-existed in the culture media. The results showed that the co-existence of 10 μM PDS had little effect on the cytotoxicity of *trans*-PtTz (Supplementary Figure S6A). Given the downregulation of PC4 by PDS takes time, we then performed *in vitro* anti-proliferative assay for *trans*-PtTz after HeLa cells were pre-treated with PDS for 24 h. The results showed that the IC_{50} of *trans*-PtTz was dramatically reduced by 4.2- and 5.5-fold subjected to pre-treatment with 2 and 10 μM PDS, respectively (Figure 5B and Supplementary Figure S6B). In both cases, the IC_{50} value of *trans*-PtTz was even slightly lower than that of cis-

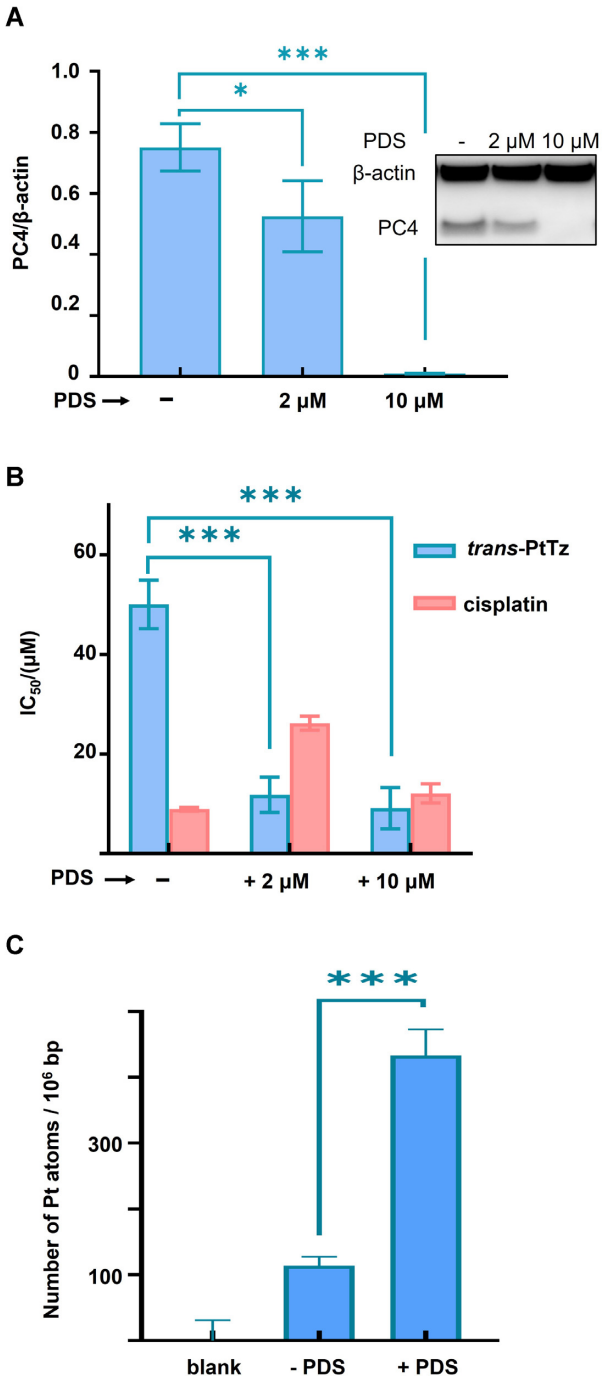

Figure 5. (**A**) Ratio of PC4 to the internal standard protein β-actin in HeLa cells without and with PDS pre-treatment measured by western blot assay ($n = 3$). The insert shows the optical density of PC4 and β-actin in a WB measurement. (**B**) IC_{50} values of *trans*-PtTz and cisplatin toward HeLa cells without and with PDS pre-treatment ($n = 3$). (**C**) The number of Pt atoms bound to 10^6 base pair measured by ICP-MS ($n = 3$) in HeLa cells treatment with 25 μM *trans*-PtTz with and without pre-treatment of 10 μM PDS. The blank represents the aqueous solution containing all reagents to prepare the samples but no DNA extract. Two-tailed unpaired Student's *t*-test was used for all statistics analysis, * indicates $P < 0.05$ and *** $P < 0.001$.

platin, one of the most widely used chemotherapeutic, of which the IC_{50} was increased slightly when the HeLa cells were pre-treated with PDS (Figure 5B and Supplementary Figure S6C), perhaps due to activation of cell cycle process by PDS (*vide supra*). Notably, there was no obvious difference between the IC_{50} of *trans*-PtTz with 2 and 10 μM PDS pre-treatment (Figure 5B). According to the western blotting data shown in Figure 5A, 2 μM PDS could only downregulate ca. 33% of PC4. Taking the moderate binding affinity of PC4 to the 1,3-*trans*-PtTz crosslinked DNA into account (42), we speculate that since PC4 is abundantly expressed in cells, 33% deletion of PC4 in HeLa cells already reduced sufficiently the binding of PC4 to damaged DNA by *trans*-PtTz, resulting significant promotion of cytotoxicity of *trans*-PtTz.

In order to further verify that the promotion of cytotoxicity of *trans*-PtTz by PDS did result from the downregulation of PC4, which might hamper the repair of *trans*-PtTz induced 1,3-crosslinked DNA lesion mediated by PC4, we used time of flight secondary ion mass spectrometry (ToF-SIMS) to image *trans*-PtTz in HeLa cells, in particular in nuclei rendered by PO_3^- ions (31), with and without PDS pretreatment. The cells were divided into three groups: blank group (cells were cultivated in the absence of both PDS and *trans*-PtTz), control group (cells were treated with 25 μM *trans*-PtTz only for 24 h) and PDS group (cells were pretreated with 10 μM PDS for 24 h and then exposed to 25 μM *trans*-PtTz for further 24 h). The resulting images showed that the platinum content as indicated by $[PtCN]^-$ (31,32) at the single cell level was higher in the PDS pre-treated cells than in the control group of cells (Figures 6A and B). The statistical results of randomly selected 20 cells in control group and PDS group also showed that platinum accumulation in the cells pre-treated by PDS was significantly higher than that in the cells of control group (Figure 6C), confirming that the pretreatment of PDS increased the accumulation of *trans*-PtTz in HeLa cells, subsequently promoting the cytotoxicity of *trans*-PtTz, most probably ascribed to reduction in the repair of platinated DNA *via* downregulating PC4 expression. Moreover, the ICP-MS measurement of Pt content in genomic DNA of large scale of HeLa cells demonstrated that the Pt content binding to DNA in HeLa cells pre-treated with PDS was 4-fold higher than that binding to DNA in the control cells (Figure 5C), further supporting that PDS pretreatment increased platination of DNA in HeLa cells by retarding the repair of platinated DNA lesion mediated by PC4, thereby promoting the cytotoxicity of *trans*-PtTz.

DISCUSSION

As mentioned earlier, PDS acting as a G4 inducer and/or stabilizer is expected to target the genes containing rich G4 potential sequences. However, the impact of PDS as a G4 inducer or binder on gene expression is very complicated. PDS can cause DNA double-strand breaks (16) and displace G4-binding proteins, for example, transcription factors (21,23). The PDS–G4 interactions can occur both in DNA and RNA, impacting oppositely on transcription and translation levels of genes (22). Our study herein confirmed that all the PDS-downregulated genes indeed have rich G4

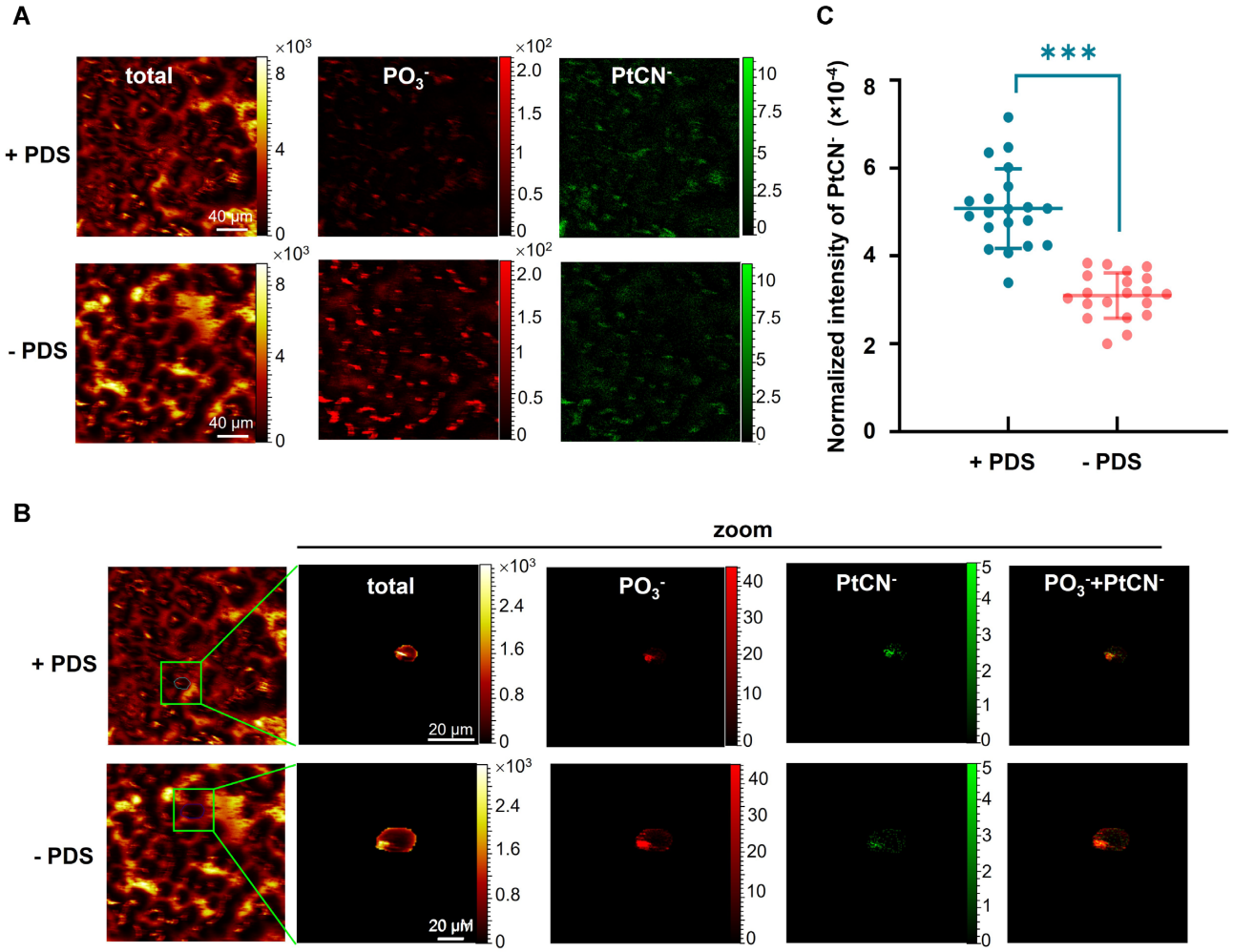

Figure 6. ToF-SIMS images of HeLa cells exposed to 25 μM *trans*-PtTz for 24 h without PDS pre-treatment (-PDS), or with 10 μM PDS pre-treatment (+PDS) for 24 h. (**A** and **B**) Images of total ions, PO_3^- and $PtCN^-$ in a 250 × 250 μm of view (A) and in a single cell (B). (**C**) The normalized intensity of $PtCN^-$ signal determined by ToF-SIMS in each HeLa cell. We randomly selected 20 cells in each group for statistic calculation, *** indicates $P < 0.001$.

forming G-rich sequences (QGRS) in their transcribed sequences and promotor regions. However, on one hand the number of QGRS in a gene is not positively correlated with the downregulation level in the expression of the gene by PDS. On the other hand, the 16 PDS-upregulated genes also contain a certain number of G4 potential sequences in both transcribed sequences and promotor regions. These results indicate that PDS induced formation and/or stabilization of G4 structures can inhibit the expression of some genes, but promote the expression of others, consistent with previous reports (22).

The high anticancer efficiency of cisplatin and the clinical ineffectiveness of its *trans*-isomer (transplatin) are considered to be a paradigm of the classic structure-activity relationship of small molecular chemical drugs. However, when one of the amine ligands in transplatin is replaced by a planar amine (L), the transplatinum complexes in type of *trans*-[$PtCl_2(NH_3)(L)$] become cytotoxic, and even have activity against cisplatin-resistant tumor cells (43,44). *Trans*-[$PtCl_2(NH_3)$(thiazole)] (*trans*-PtTz) is such a complex, but its cytotoxicity is still much lower than that of cisplatin. Like cisplatin, *trans*-PtTz was believed to target DNA. However, unlike cisplatin which forms mainly 1,2-intrastrand crosslinked DNA adducts, *trans*-PtTz produces monofunctional (30–40%), 1,3-intrastrand crosslinked (20–40%) and 1,2-interstrand crosslinked DNA adducts (30–40%) (41). Unfortunately, so far which form of DNA damage induced by *trans*-PtTz plays a major role in its cytotoxicity has remained unclear.

Our previous work revealed that the human nuclear positive cofactor PC4 recognized and specifically bound to 1,3-intrastrand crosslinked DNA by *trans*-PtTz (36). However, the biological implication and consequence of this unique recognition and interaction between PC4 and 1,3-*trans*-PtTz crosslinked DNA have not been deciphered so far. PC4 is an abundant multifunctional nuclear protein, and plays important roles in various cellular processes such as transcription, DNA repair and replication, chromatin organization and cell cycle progression (45–49). PC4 usually forms a homodimer to host single-stranded DNA (ssDNA) at DNA damage sites, recruiting various proteins, in particular DNA repair proteins, to exert their functions (50–52).

DNA damage repair is the main molecular mechanism of resistance to platinum anticancer drugs such as cisplatin, through which the DNA repair machinery, consisting of DNA lesion recognition protein and nucleotide excision repair (NER) proteins, e.g. XPA and ERCC1 as DNA damage recognizer and NER protein, respectively, plays a crucial role in the repair of cisplatin damaged DNA (53). When the expression of XPA and ERCC1 were down-regulated, the resistance of cancer cells to cisplatin was significantly reduced (54,55). Our studies herein unambiguously unraveled that the PDS induced downregulation of PC4 promoted the cytotoxicity of *trans*-PtTz toward HeLa cells. Combining with the results obtained by western blotting, SIMS and ICP-MS assays, we concluded that it was PDS-induced reduction in expression of PC4 that promoted the cytotoxicity of *trans*-PtTz due to retarding the PC4-mediated repair of the DNA lesion induced by *trans*-PtTz. In other words, PC4 binds to the 1,3-transplatinated DNA to trigger DNA repair, which as a consequence reduces the cytotoxicity of *trans*-PtTz. With regard to this, other DNA repair inhibitors may be expected to show similar enhancement of cytotoxicity of *trans*-PtTz.

Given that cisplatin mainly causes 1,2-intrastrand cross-linked DNA lesion, leading to cell death and apoptosis (56), *trans*-PtTz which causes DNA damages by forming 1,3-intranstrand/1,2-interatrand DNA adducts and monofunctional DNA adducts, was shown to have no cross-resistance with cisplatin (43,44). However, the relative low cytotoxicity of *trans*-PtTz compared to cisplatin limits its further application. With regard to this, the significantly promotion of cytotoxicity of *trans*-PtTz by PDS provides a unique solution to circumvent resistance against cisplatin which is a major restraint for cisplatin use in clinic. Our study herein also implicates a new strategy for the rational design of novel multi-targeting platinum anticancer drugs via conjugating PDS as a ligand to the coordination scaffold of transplatin or encapsulating *trans*-PtTz and PDS into a controllably released drug carrier system.

In summary, in the present work we discovered for the first time that the G4 stabilizer and inducer, PDS, remarkably down-regulated 22 proteins in HeLa cells, while at the same time upregulating significantly 16 proteins related to regulation of cell cycle and cellular component organization. Importantly, PDS was demonstrated to downregulate the expression of human nuclear positive cofactor PC4, dramatically promoting the cytotoxicity of *trans*-PtTz toward HeLa cells. Further studies revealed that PDS induced downregulation of PC4 retarded the repair of *trans*-PtTz induced 1,3-intrastand DNA lesion mediated by PC4, and increased accumulation of *trans*-PtTz in cells, thereby enhancing the cytotoxicity of this complex. This finding presents a novel strategy for designing new multi-targeting platinum anticancer drugs to battle drug resistance to cisplatin.

DATA AVAILABILITY

The mass spectrometry proteomics data have been deposited to the ProteomeXchange Consortium *via* the PRIDE (57) partner repository with the dataset identifier PXD029521.

SUPPLEMENTARY DATA

Supplementary Data are available at NAR Online.

ACKNOWLEDGEMENTS

We thank Professor Yu Zhang at National Institute of Biological Sciences for the Cas9-SunTag plasmids and Professor Yangzhong Liu at University of Science and Technology of China for *trans*-PtTz as gifts. Also many thanks to Professors Xiaohong Fang and Ming Wang at Institute of Chemistry, Chinese Academy of Sciences for helps in Western Blotting assays.

FUNDING

National Natural Science Foundation of China [21927804, 21635008, 21790390, 21790392, 21127901, 22004121]; National Key Research and Development Program of China [2018YFA0800903]; China Postdoctoral Science Foundation [2020M680675]; Youth Innovation Promotion Association of Chinese Academy of Sciences [2017051 to Y.Z.]; BMS [2019BMS20012 to T.F.]. Funding for open access charge: National Natural Science Foundation of China [21927804].

Conflict of interest statement. We have documented the combined use of the studied compounds, pyridostatin and *trans* [$PtCl_2(NH_3)$(thiazole)], in this work for cancer therapy in a Chinese patent application.

REFERENCES

1. Hansel-Hertsch,R., Beraldi,D., Lensing,S.V., Marsico,G., Zyner,K., Parry,A., Di Antonio,M., Pike,J., Kimura,H., Narita,M. *et al.* (2016) G-quadruplex structures mark human regulatory chromatin. *Nat. Genet.*, **48**, 1267–1272.
2. Guedin,A., Gros,J., Alberti,P. and Mergny,J.-L. (2010) How long is too long? Effects of loop size on G-quadruplex stability. *Nucleic Acids Res.*, **38**, 7858–7868.
3. Bedrat,A., Lacroix,L. and Mergny,J.L. (2016) Re-evaluation of G-quadruplex propensity with G4Hunter. *Nucleic Acids Res.*, **44**, 1746–1759.
4. Chambers,V.S., Marsico,G., Boutell,J.M., Di Antonio,M., Smith,G.P. and Balasubramanian,S. (2015) High-throughput sequencing of DNA G-quadruplex structures in the human genome. *Nat. Biotechnol.*, **33**, 877–881.
5. Hansel-Hertsch,R., Spiegel,J., Marsico,G., Tannahill,D. and Balasubramanian,S. (2018) Genome-wide mapping of endogenous G-quadruplex DNA structures by chromatin immunoprecipitation and high-throughput sequencing. *Nat. Protoc.*, **13**, 551–564.
6. Cogoi,S. and Xodo,L.E. (2006) G-quadruplex formation within the promoter of the KRAS proto-oncogene and its effect on transcription. *Nucleic Acids Res.*, **34**, 2536–2549.
7. Cox,A.D., Fesik,S.W., Kimmelman,A.C., Luo,J. and Der,C.J. (2014) Drugging the undruggable RAS: mission possible?*Nat. Rev. Drug Discov.*, **13**, 828–851.
8. Miyazaki,T., Pan,Y., Joshi,K., Purohit,D., Hu,B., Demir,H., Mazumder,S., Okabe,S., Yamori,T., Viapiano,M. *et al.* (2012) Telomestatin impairs glioma stem cell survival and growth through the disruption of telomeric G-Quadruplex and inhibition of the Proto-oncogene, c-Myb. *Clin. Cancer Res.*, **18**, 1268–1280.
9. Edling,C.E. and Hallberg,B. (2007) c-Kit - A hematopoietic cell essential receptor tyrosine kinase. *Int. J. Biochem. Cell Biol.*, **39**, 1995–1998.
10. Radha,G. and Raghavan,S.C. (2017) BCL2: a promising cancer therapeutic target. *Biochim. Biophys. Acta Rev. Cancer*, **1868**, 309–314.

11. Siddiqui-Jain,A., Grand,C.L., Bearss,D.J. and Hurley,L.H. (2002) Direct evidence for a G-quadruplex in a promoter region and its targeting with a small molecule to repress c-MYC transcription. *Proc. Natl. Acad. Sci. USA*, **99**, 11593–11598.
12. Gonzalez,V. and Hurley,L.H. (2010) The c-MYC NHE III1: function and regulation. *Annu. Rev. Pharmacol. Toxicol.*, **50**, 111–129.
13. Rodriguez,R., Muller,S., Yeoman,J.A., Trentesaux,C., Riou,J.F. and Balasubramanian,S. (2008) A novel small molecule that alters shelterin integrity and triggers a DNA-Damage response at telomeres. *J. Am. Chem. Soc.*, **130**, 15758–15759.
14. Chung,W.J., Heddi,B., Hamon,F., Teulade-Fichou,M.P. and Phan,A.T. (2014) Solution structure of a G-quadruplex bound to the bisquinolinium compound Phen-DC3. *Angew. Chem. Int. Ed.*, **53**, 999–1002.
15. Burger,A.M., Dai,F.P., Schultes,C.M., Reszka,A.P., Moore,M.J., Double,J.A. and Neidle,S. (2005) The G-quadruplex-interactive molecule BRACO-19 inhibits tumor growth, consistent with telomere targeting and interference with telomerase function. *Cancer Res.*, **65**, 1489–1496.
16. Rodriguez,R., Miller,K.M., Forment,J.V., Bradshaw,C.R., Nikan,M., Britton,S., Oelschlaegel,T., Xhemalce,B., Balasubramanian,S. and Jackson,S.P. (2012) Small-molecule-induced DNA damage identifies alternative DNA structures in human genes. *Nat. Chem. Biol.*, **8**, 301–310.
17. Salvati,E., Scarsella,M., Porru,M., Rizzo,A., Iachettini,S., Tentori,L., Graziani,G., D'Incalci,M., Stevens,M.F.G., Orlandi,A. *et al.* (2010) PARP1 is activated at telomeres upon G4 stabilization: possible target for telomere-based therapy. *Oncogene*, **29**, 6280–6293.
18. Koirala,D., Dhakal,S., Ashbridge,B., Sannohe,Y., Rodriguez,R., Sugiyama,H., Balasubramanian,S. and Mao,H.B. (2011) A single-molecule platform for investigation of interactions between G-quadruplexes and small-molecule ligands. *Nat. Chem.*, **3**, 782–787.
19. Marsico,G., Chambers,V.S., Sahakyan,A.B., McCauley,P., Boutell,J.M., Di Antonio,M. and Balasubramanian,S. (2019) Whole genome experimental maps of DNA G-quadruplexes in multiple species. *Nucleic Acids Res.*, **47**, 3862–3874.
20. Moruno-Manchon,J.F., Lejault,P., Wang,Y.X., McCauley,B., Honarpisheh,P., Scheihing,D.A.M., Singh,S., Dang,W.W., Kim,N., Urayama,A. *et al.* (2020) Small-molecule G-quadruplex stabilizers reveal a novel pathway of autophagy regulation in neurons. *Elife*, **9**, e52283.
21. Li,L., Williams,P., Ren,W.D., Wang,M.Y., Gao,Z., Miao,W.L., Huang,M., Song,J.K. and Wang,Y.S. (2021) YY1 interacts with guanine quadruplexes to regulate DNA looping and gene expression. *Nat. Chem. Biol.*, **17**, 161–168.
22. He,X.M., Yuan,J. and Wang,Y.S. (2021) G3BP1 binds to guanine quadruplexes in mRNAs to modulate their stabilities. *Nucleic Acids Res.*, **49**, 11323–11336.
23. Li,L., Williams,P., Gao,Z. and Wang,Y.S. (2020) VEZF1-guanine quadruplex DNA interaction regulates alternative polyadenylation and detyrosinase activity of VASH1. *Nucleic Acids Res.*, **48**, 11994–12003.
24. Gilbert,J.A., Blaser,M.J., Caporaso,J.G., Jansson,J.K., Lynch,S.V. and Knight,R. (2018) Current understanding of the human microbiome. *Nat. Med.*, **24**, 392–400.
25. Ding,L., Bailey,M.H., Porta-Pardo,E., Thorsson,V., Colaprico,A., Bertrand,D., Gibbs,D.L., Weerasinghe,A., Huang,K.L., Tokheim,C. *et al.* (2018) Perspective on oncogenic processes at the end of the beginning of cancer genomics. *Cell*, **173**, 305–320.
26. Mackay,F.S., Moggach,S.A., Collins,A., Parsons,S. and Sadler,P.J. (2009) Photoactive trans ammine/amine diazido platinum(IV) complexes. *Inorg. Chim. Acta*, **362**, 811–819.
27. Alderden,R.A., Hall,M.D. and Hambley,T.W. (2006) The discovery and development of cisplatin. *J. Chem. Educ.*, **83**, 728–734.
28. Biffi,G., Tannahill,D., McCafferty,J. and Balasubramanian,S. (2013) Quantitative visualization of DNA G-quadruplex structures in human cells. *Nat. Chem.*, **5**, 182–186.
29. Tanenbaum,M.E., Gilbert,L.A., Qi,L.S., Weissman,J.S. and Vale,R.D. (2014) A protein-tagging system for signal amplification in gene expression and fluorescence imaging. *Cell*, **159**, 635–646.
30. Brewis,N., Phelan,A., Webb,J., Drew,J., Elliott,G. and O'Hare,P. (2000) Evaluation of VP22 spread in tissue culture. *J. Virol.*, **74**, 1051–1056.
31. Lin,Y., Wu,K., Jia,F.F., Chen,L., Wang,Z.Y., Zhang,Y.Y., Luo,Q., Liu,S.Y., Qi,L.Y., Li,N. *et al.* (2021) Single cell imaging reveals cisplatin regulating interactions between transcription (co)factors and DNA. *Chem. Sci.*, **12**, 5419–5429.
32. Jia,F.F., Wang,J., Zhao,Y., Zhang,Y.Y., Luo,Q., Qi,L.Y., Hou,Y.Z., Du,J. and Wang,F.Y. (2020) In situ visualization of proteins in single cells by Time-of-Flight-Secondary ion mass spectrometry coupled with genetically encoded chemical tags. *Anal. Chem.*, **92**, 15517–15525.
33. Spiegel,J., Cuesta,S.M., Adhikari,S., Hansel-Hertsch,R., Tannahill,D. and Balasubramanian,S. (2021) G-quadruplexes are transcription factor binding hubs in human chromatin. *Genome Biol.*, **22**, 117–131.
34. Kikin,O., D'Antonio,L. and Bagga,P.S. (2006) QGRS mapper: a web-based server for predicting G-quadruplexes in nucleotide sequences. *Nucleic Acids Res.*, **34**, W676–W682.
35. Mortusewicz,O., Roth,W., Li,N., Cardoso,M.C., Meisterernst,M. and Leonhardt,H. (2008) Recruitment of RNA polymerase II cofactor PC4 to DNA damage sites. *J. Cell Biol.*, **183**, 769–776.
36. Du,Z.F., Luo,Q., Yang,L.P., Bing,T., Li,X.C., Guo,W., Wu,K., Zhao,Y., Xiong,S.X., Shangguan,D.H. *et al.* (2014) Mass spectrometric proteomics reveals that nuclear protein positive cofactor PC4 selectively binds to cross-linked DNA by a trans-Platinum anticancer complex. *J. Am. Chem. Soc.*, **136**, 2948–2951.
37. Caldwell,R.B., Braselmann,H., Schoetz,U., Heuer,S., Scherthan,H. and Zitzelsberger,H. (2016) Positive cofactor 4 (PC4) is critical for DNA repair pathway re-routing in DT40 cells. *Sci. Rep.*, **6**, 28890–28903.
38. Mortusewicz,O., Evers,B. and Helleday,T. (2016) PC4 promotes genome stability and DNA repair through binding of ssDNA at DNA damage sites. *Oncogene*, **35**, 761–770.
39. Batta,K., Yokokawa,M., Takeyasu,K. and Kundu,T.K. (2009) Human transcriptional coactivator PC4 stimulates DNA end joining and activates DSB repair activity. *J. Mol. Biol.*, **385**, 788–799.
40. Bierbach,U., Qu,Y., Hambley,T.W., Peroutka,J., Nguyen,H.L., Doedee,M. and Farrell,N. (1999) Synthesis, structure, biological activity, and DNA binding of platinum(ii) complexes of the type trans-[PtCl(2)(NH(3))L] (L = planar nitrogen base). Effect of l and cis/trans isomerism on sequence specificity and unwinding properties observed in globally platinated DNA. *Inorg. Chem.*, **38**, 3535–3542.
41. Marini,V., Christofis,P., Novakova,O., Kasparkova,J., Farrell,N. and Brabec,V. (2005) Conformation, protein recognition and repair of DNA interstrand and intrastrand cross-links of antitumor trans-[PtCl2(NH3)(thiazole)]. *Nucleic Acids Res.*, **33**, 5819–5828.
42. Du,Z., Luo,Q., Yang,L., Bing,T., Li,X., Guo,W., Wu,K., Zhao,Y., Xiong,S., Shangguan,D. *et al.* (2014) Mass spectrometric proteomics reveals that nuclear protein positive cofactor PC4 selectively binds to cross-linked DNA by a trans-Platinum anticancer complex. *J. Am. Chem. Soc.*, **136**, 2948–2951.
43. Brabec,V. (2002) DNA modifications by antitumor platinum and ruthenium compounds: their recognition and repair. *Prog. Nucleic Acid Res. Mol. Biol.*, **71**, 1–68.
44. Perez,J.M., Fuertes,M.A., Alonso,C. and Navarro-Ranninger,C. (2000) Current status of the development of trans-platinum antitumor drugs. *Crit. Rev. Oncol. Hematol.*, **35**, 109–120.
45. Garavís,M. and Calvo,O. (2017) Sub1/PC4, a multifaceted factor: from transcription to genome stability. *Curr. Genet.*, **63**, 1023–1035.
46. Tavenet,A., Suleau,A., Dubreuil,G., Ferrari,R., Ducrot,C., Michaut,M., Aude,J.-C., Dieci,G., Lefebvre,O., Conesa,C. *et al.* (2009) Genome-wide location analysis reveals a role for sub1 in RNA polymerase III transcription. *Proc. Natl. Acad. Sci. USA*, **106**, 14265–14270.
47. Pan,Z.Q., Ge,H., Amin,A.A. and Hurwitz,J. (1996) Transcription-positive cofactor 4 forms complexes with HSSB (RPA) on single-stranded DNA and influences HSSB-dependent enzymatic synthesis of simian virus 40 DNA. *J. Biol. Chem.*, **271**, 22111–22116.
48. Wang,J.Y., Sarker,A.H., Cooper,P.K. and Volker,M.R. (2004) The single-strand DNA binding activity of human PC4 prevents mutagenesis and killing by oxidative DNA damage. *Mol. Cell. Biol.*, **24**, 6084–6093.
49. Ge,H. and Roeder,R.G. (1994) Purification, cloning, and characterization of a human coactivator, PC4, that mediates transcriptional activation of class II genes. *Cell*, **78**, 513–523.

50. Brandsen,J., Werten,S., van der Vliet,P.C., Meisterernst,M., Kroon,J. and Gros,P. (1997) C-terminal domain of transcription cofactor PC4 reveals dimeric ssDNA binding site. *Nat. Struct. Biol.*, **4**, 900–903.
51. Werten,S. and Moras,D. (2006) A global transcription cofactor bound to juxtaposed strands of unwound DNA. *Nat. Struct. Mol. Biol.*, **13**, 181–182.
52. Hyjek-Składanowska,M., Vickers,T.A., Napiórkowska,A., Anderson,B.A., Tanowitz,M., Crooke,S.T., Liang,X.-h., Seth,P.P. and Nowotny,M. (2020) Origins of the increased affinity of phosphorothioate-modified therapeutic nucleic acids for proteins. *J. Am. Chem. Soc.*, **142**, 7456–7468.
53. Brabec,V. and Kasparkova,J. (2005) Modifications of DNA by platinum complexes - Relation to resistance of tumors to platinum antitumor drugs. *Drug Resist. Update*, **8**, 131–146.
54. Wu,X.M., Fan,W., Xu,S.W. and Zhou,Y.K. (2003) Sensitization to the cytotoxicity of cisplatin by transfection with nucleotide excision repair gene xeroderma pigmentosun group a antisense RNA in human lung adenocarcinoma cells. *Clin. Cancer Res.*, **9**, 5874–5879.
55. Selvakumaran,M., Pisarcik,D.A., Bao,R., Yeung,A.T. and Hamilton,T.C. (2003) Enhanced cisplatin cytotoxicity by disturbing the nucleotide excision repair pathway in ovarian cancer cell lines. *Cancer Res.*, **63**, 1311–1316.
56. Jung,Y.W. and Lippard,S.J. (2007) Direct cellular responses to platinum-induced DNA damage. *Chem. Rev.*, **107**, 1387–1407.
57. Perez-Riverol,Y., Csordas,A., Bai,J.W., Bernal-Llinares,M., Hewapathirana,S., Kundu,D.J., Inuganti,A., Griss,J., Mayer,G., Eisenacher,M. *et al.* (2019) The PRIDE database and related tools and resources in 2019: improving support for quantification data. *Nucleic Acids Res.*, **47**, D442–D450.